

Active chemo-mechanical solitons

L. Truskinovsky

PMMH, CNRS – UMR 7636, CNRS, ESPCI Paris, PSL Research University, 10 rue Vauquelin, 75005 Paris, France

G. Zurlo

School of Mathematical and Statistical Sciences, University of Galway, University Road, Galway, Ireland

In many biological systems localized mechanical information is transmitted by mechanically neutral chemical signals. Typical examples include contraction waves in acto-myosin cortex at cellular scale and peristaltic waves at tissue level. In such systems, chemical activity is transformed into mechanical deformation by distributed motor-type mechanisms represented by continuum degrees of freedom. To elucidate the underlying principles of chemo-mechanical coupling, we here present the simplest example, involving directional motion of a localized solitary wave in a distributed mechanical system, guided by a purely chemical cue. Our main result is that mechanical signals can be driven by chemical activity in a highly efficient manner.

INTRODUCTION

While molecular biology and biochemistry clearly play dominant roles in biological processes, mechanics has recently emerged as another crucial co-player [1–4]. However, how chemically generated microscopic forces are transformed into a functional mechanical deformation at the macroscale still remains opaque [5, 6].

Of particular interest in this respect are the mechanisms of directional transmission of localized mechanical information by mechanically-neutral chemical signals. For instance, cardiac muscles have the ability to actively generate functional dynamic contractions [7], fluid propulsion of many cellular organisms is achieved by deformation waves [8, 9], fronts of cytoskeletal reinforcement were observed during epithelial monolayer expansion [10, 11] and finally peristalsis in digestive tract performs the most remarkable directed mechanical activity [12–14].

It is known that the inner working of the implied chemical machinery can be modeled by various excitable reaction-diffusion systems [15]. However, it remains unclear how a fueling chemical signal can transform into a propagating localized wave-like deformation field, and how such chemo-mechanical system can attain the observed high levels of energetic efficiency [16–19].

To elucidate the underlying principles of chemo-mechanical coupling we present in this paper the simplest example of a directional motion of a solitary wave in a distributed mechanical system driven by a mechanically neutral signal of chemical origin.

We build on a previous work where other systems displaying active chemo-mechanical coupling have been extensively studied, see for instance, [20–27]. In particular, various models have been proposed showing that elastic instabilities can be produced and dynamically regulated by excitable reaction-diffusion systems [24, 28–32].

In this paper we are concerned with a particular aspect of such dynamic actuation. Specifically, we show that chemo-mechanical driving of localized solitary waves (solitons, for simplicity) can be mechanically efficient in the sense that the

mechanical energy needed to activate the pulse at the leading edge can be transported from trailing edge where it is released due to the the pulse closure. As we show, such self-sustaining machinery can indeed be operative due to the existence of a mechanism of an internal energy transport through wave dispersion [33–35]. In this case mechanical signal can propagate without taking any energy from the triggering chemical signal due to an on board energy-harvesting.

To highlight ideas we consider in this exploratory paper only a purely mechanical side of the corresponding energy transport mechanism without invoking in any detail the underlying chemical machinery [36–39]. Specifically, we restore to the simplest phenomenological approach in the description of active stress generation [40, 41]. Using such stylized framework, we show that a mechanical solitary wave can be indeed generated chemically even in a *linear* mechanical system. Moreover, we show that the chemo-mechanical coupling in such model is maximally efficient, which means that the active chemical system does not need to expend energy to sustain the mechanical signal beyond what is needed to maintain chemical activation.

A realistic example of the implied chemo-mechanical coupling can be found, for instance, in [42] where the authors present an experimental realization of the propagating reaction-diffusion fronts generated by Belousov-Zhabotinsky reaction which can induce localized deformation in a gel. Similarly, in [43] the authors recreate *in vitro* the actomyosin cytoskeleton and show that some of its buckling type shape deformations can be driven actively by myosin motors. *Vis-a-vis* our schematic model, the propagation of motor-induced activity can be viewed as the analog of our chemical signal which also generates pre-stress responsible for dynamic buckling. More elaborate chemo-elastic interactions are discussed, for instance, in [44] and in such perspective, our minimal formulation is intentionally schematic. However, due to its full analytical tractability, the proposed model allowed us to reveal a novel fundamental mechanism of dispersive energy transport expected to be operative in such active systems.

Our main technical tool is the theory of dispersive systems allowing dynamical energy transport [45]. We build on the

ideas developed in the theory of configurational defects in crystal lattices [46, 47], which can produce lattice scale energy radiation but can be also dynamically guided by lattice waves [47, 48]. The main goal of this study is to show that similar dispersion-induced mechanisms can ensure that the energy generated by chemically activated sources can be fully transmitted to chemically supported sinks which would then make a loss-free propagation of mechanical information possible.

THE MODEL

In the interest of analytical transparency, we consider only a 1D dynamic problem with $u(x, t)$ denoting a scalar displacement field (longitudinal or transverse), x being a reference coordinate. Having in mind the elastic softness of the modeled biological prototypes, we assume that the system is elastically degenerate (infinitely stretchable), which brings into the theory a continuous symmetry. The corresponding Goldstone (soft) mode is described by the strain variable u_x , where the subscript indicates partial derivative. When the strain is a slowly varying inhomogeneous field, the corresponding small energy cost can be captured by a quadratic function of strain gradients, meaning that the implied infinitely soft material still carries gradient (bending) rigidity. The corresponding free energy is then

$$\int \frac{\kappa}{2} u_{xx}^2 dx$$

where κ is the bending modulus, and subscripts denote partial derivatives, e.g., $u_x \equiv \partial u / \partial x$, $u_{xx} \equiv \partial^2 u / \partial x^2$, etc. Such energy emerges, for instance, in continuum representation of a deliberately minimalistic pantographic structure, as shown in Fig.1. It is built of inextensible but flexible beams, connected through ideal pivots. While the structure is floppy, showing zero stiffness when it is deformed uniformly [49], inhomogeneous deformations are energetically penalized due to nonzero bending rigidity of the beams [50]. More complex examples of bending-dominated structures can be found in the theory of high contrast elastic composites [51, 52]; in such systems the second order elasticity appears already at the leading order in the homogenization (continuum) limit, which justifies our choice of the elastic energy.

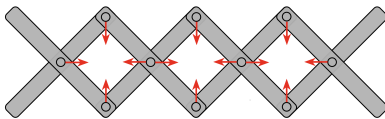


Figure 1. Mechanical model of pantograph with integrated active pulling (contractile) elements represented by red arrows. While the underconstrained pantograph structure is not rigid and contains a longitudinal soft mode, the presence of active elements makes it overconstrained.

In Fig. 1 we also show that the under-constrained pantograph structure can be stabilized through the pre-stress by active elements which eliminate the corresponding soft (floppy)

modes. To effectively incorporate such elements into the model, we need to account for a term in the energy of the form

$$\int \sigma_a(x, t) u_x dx.$$

We further assume that the (pre)stress σ_a is piecewise constant spin variable taking three values $\{\sigma_0, 0, -\sigma_0\}$, intended to represent active stretching, deactivation and active compression, accordingly. In Fig.1 we illustrate the fact that all of these states can be achieved by using antagonistic, purely contractile elements; it also shows that contraction can be amplified by the arrangement which turns small microscopic deformations into large macroscopic movements [53].

To allow for dispersive non-dissipative energy transport in the model we also need to account for (pseudo)inertia by introducing into the energy the term

$$\int \frac{\rho}{2} u_t^2 dx.$$

The interpretation of such term as the actual kinetic energy may still make sense due to our choice of ultra-soft stretching elasticity, which turns into supersonic even for extremely slow mechanical signals. However, in physiological setting, the apparent mass density ρ should be rather viewed as bringing into the constitutive model an internal time scale, describing the functional, activity-induced, time delay. Such delay was found relevant, for instance, in the description of the activity of molecular motors, stretch receptors, ERK waves, etc. [10, 11, 54].

VARIATIONAL FORMULATION

In view of the conservative nature of the mechanical part of the ensuing model, it will be convenient to obtain the corresponding dynamic equations and boundary conditions using the variational Hamilton (action) principle. The Lagrange function in our case has the form

$$L = \frac{1}{2} \rho u_t^2 - \sigma_a u_x - \frac{1}{2} \kappa u_{xx}^2 \quad (1)$$

where the inhomogeneous controls $\sigma_a(x, t)$ are assumed to be given. It will be also convenient to first rewrite the problem in more general terms by introducing the variables $q^1 = x$ and $q^2 = t$, and presenting the displacement field in the form $u(q^\alpha)$, with Greek indices $\alpha, \beta, \gamma = 1, 2$ in the remainder of this section. The corresponding action functional is

$$\mathcal{L} = \int_{\Omega} L(q^\alpha, u_\alpha, u_{\alpha\beta}) dq^1 dq^2 \quad (2)$$

where we introduced a two-dimensional *space-time* domain Ω describing the evolution of a body between two time instants [55], and where again $u_\alpha = \partial u / \partial q^\alpha$. The corresponding

Euler-Lagrange equations, representing the balance of linear momentum, take the form

$$\frac{\partial}{\partial q^\alpha} \left(\frac{\delta L}{\delta u_\alpha} \right) = 0$$

where

$$\frac{\delta L}{\delta u_\alpha} = \frac{\partial L}{\partial u_\alpha} - \frac{\partial}{\partial q^\beta} \left(\frac{\partial L}{\partial u_{\alpha\beta}} \right)$$

is the variational derivative and the summation over repeated indexes is implied. In our special case we obtain the linear equation

$$\rho u_{tt} = \sigma_x$$

where

$$\sigma = \sigma_a - \kappa u_{xxx}.$$

Suppose next that the domain Ω contains a propagating surface Σ where the function $\sigma_a(x, t)$ suffers a jump discontinuity, while it remains constant outside. On Σ the dependence of L on q^α is discontinuous, which leads to the possibility of energy sources or sinks. It is natural to assume that the particle trajectories on Σ are continuous, so that

$$[u] = 0$$

where

$$[f] = f^+ - f^-$$

with the superscripts \pm denoting the limiting values of f . To ensure finiteness of the energy it is also natural to assume that the particle trajectories are smooth,

$$[u_x] = 0.$$

On Σ the stationarity of the action \mathcal{L} imposes the conditions representing continuity of linear momentum and hypertractions (moments) on the jump [56, 57]:

$$[\frac{\delta L}{\delta u_\alpha}] n_\alpha = 0 \quad (3)$$

and

$$[\frac{\delta L}{\delta u_{\alpha\beta}}] n_\alpha n_\beta = 0 \quad (4)$$

where n_α is the unit vector normal to Σ facing the $+$ direction. Note also that mass balance on Σ is guaranteed by the kinematic compatibility condition

$$[u_\alpha] = \mu n_\alpha$$

where μ is a scalar. The spatial n_x and temporal n_t components of the normal vector to Σ are related through

$$n_t = -n_x D$$

where D is the normal velocity of the discontinuity, and we can always assume that $n_x = 1$. Therefore, the jump conditions (3,4) reduce to

$$[\sigma + \varrho D u_t] = 0 \quad (5)$$

and

$$[m] = 0. \quad (6)$$

respectively, where we introduced a special notation for the moments (hypertractions)

$$m = \kappa u_{xx}. \quad (7)$$

Furthermore, eliminating μ we obtain the relation

$$D [u_x] + [u_t] = 0$$

requiring that on Σ not only the strain u_x , but also the velocity field u_t must be continuous.

As we have already mentioned, on a surfaces of discontinuity Σ , one can expect sources or sinks of energy. To find the rate of energy release (absorption) on such jump discontinuities, we need to assess the singular behavior on Σ of the energy momentum tensor [58, 59]

$$\tau_\beta^\alpha = L \delta_\beta^\alpha - u_\beta \frac{\partial L}{\partial u_\alpha} - u_{\gamma\beta} \frac{\partial L}{\partial u_{\gamma\alpha}} \quad (8)$$

where δ_β^α is the Kronecker symbol. Specifically, the temporal component of τ_β^α controls the energy balance. Thus if we can use Noether identity

$$\frac{\partial \tau_\beta^\alpha}{\partial q^\alpha} = 0. \quad (9)$$

and then take $\beta = 2$ we obtain the equation

$$w_t + \mathcal{J}_x = 0,$$

where

$$w = \frac{1}{2} \rho u_t^2 + \sigma_a u_x + \frac{1}{2} \kappa u_{xx}^2$$

is the energy density and

$$\mathcal{J} = -\sigma u_t - \kappa u_{xt} u_{xx}$$

is the flux. To compute a singular energy release (absorption) on the surface of discontinuity Σ we need to compute the normal projection

$$\mathcal{D} = [\tau_2^\alpha] n_\alpha. \quad (10)$$

In view of the imposed continuity conditions the rate of dissipation at a jump is then

$$\mathcal{D} = D [\sigma_a] \{u_x\} \quad (11)$$

where we introduced the average

$$\{f\} = \frac{1}{2} (f^+ + f^-).$$

DIRECT FORMULATION

In view of a somewhat abstract nature of the variational approach, it is instructive to consider in parallel a more conventional continuum mechanical formulation of the same problem which allows one to recover the same relations but in a more pedestrian setting. We won't aim at recovering the whole classical construction from scratch but only focus on the most nontrivial aspect of the problem related to jump discontinuities.

To be more specific, consider directly a 1D problem and set it in a generic spatial domain $\mathcal{C} = (0, L)$ where we directly define the displacements field $u = u(x, t)$.

We build our discussion around the expression for the rate of change/release of the total energy

$$\mathcal{E} = \int_{\mathcal{C}} w \, dx.$$

For reasons to become clear later, we will consider a slightly more general formulation of the model based on the energy density of the form

$$w = \frac{1}{2} \varrho u_t^2 + \frac{1}{2} E u_x^2 + \frac{1}{2} \kappa u_{xx}^2 + \sigma_a u_x.$$

In addition to the nonclassical bending elasticity term, it now includes also a stretching elasticity term characterized by the energy

$$\int \frac{1}{2} E u_x^2 \, dx$$

where E is the stretching modulus.

Suppose next that the location of the surface of gradient discontinuity Σ is prescribed by the function $\zeta(t)$ so that $D = \zeta_t$. We obtain

$$\mathcal{E}_t = \int_{\mathcal{C}} (\varrho u_{tt} - \hat{\sigma}_x) u_t \, dx - [\mathcal{J}]_{\partial \mathcal{C}} - [Dw - \mathcal{J}]_{\zeta(t)} \quad (12)$$

where now the stress in the system is

$$\hat{\sigma} = \sigma_a + E u_x - \kappa u_{xxx}$$

and the energy flux is defined as

$$\mathcal{J} = -\hat{\sigma} u_t - \kappa u_{xx} u_{xt}. \quad (13)$$

We assume for simplicity that $u = u_x = 0$ at the external boundary of the body $\partial \mathcal{C}$ so that $u_t = u_{xt} = 0$ as well. Then $[\mathcal{J}]_{\partial \mathcal{C}} = 0$ and there is no outside flux of energy.

Away from discontinuity, balance of momentum is satisfied

$$\varrho u_{tt} - \hat{\sigma}_x = 0. \quad (14)$$

Note next that the jump term in (12) can be rewritten as

$$\begin{aligned} [Dw - \mathcal{J}] &= \varrho D [u_t] \{u_t\} + D \kappa \{u_{xx}\} [u_{xx}] \\ &\quad + D E \{u_x\} [u_x] + E [u_x] \{u_t\} + E \{u_x\} [u_t] \\ &\quad + D [\sigma_a] \{u_x\} + D \{\sigma_a\} [u_x] \\ &\quad + \kappa [u_{xx}] \{u_{xt}\} + \kappa [u_{xt}] \{u_{xx}\} \\ &\quad + [\sigma_a - \kappa u_{xxx}] \{u_t\} + \{\sigma_a - \kappa u_{xxx}\} [u_t] \end{aligned} \quad (15)$$

As in our variational analysis we assume that on jump discontinuities the displacement is continuous, $[u] = 0$, and therefore $[u_t] + D [u_x] = 0$. Because we have similarly assumed that $[u_x] = 0$, we also have $[u_t] = 0$. Furthermore, by time differentiation of $[u_x] = u_x^+ (\zeta(t), t) - u_x^- (\zeta(t), t) = 0$, we obtain that necessarily

$$[u_{xt} + D u_{xx}] = 0.$$

To imitate our variational setting we further assume that the corresponding tractions $\hat{\sigma}$ and moments m are continuous on the jump discontinuity, so that $[\hat{\sigma}] = 0$ and $[m] = 0$. By collecting all the jump conditions,

$$[u] = 0, \quad [u_x] = 0, \quad [u_{xx}] = 0, \quad [\sigma_a - \kappa u_{xxx}] = 0. \quad (16)$$

Finally, when using these jump conditions into (15), we find that the dissipation at every jump set equals

$$\mathcal{D} = -\mathcal{E}_t = D [\sigma_a] \{u_x\} \quad (17)$$

which expectedly agrees with (11). Note that if the rate of energy release is computed over an arbitrary region (a, b) that does not contain discontinuities, we obtain

$$\int_a^b (\hat{w}_t + \hat{\mathcal{J}}_x) \, dx = \int_a^b (\varrho u_{tt} - \hat{\sigma}_x) u_t \, dx = 0 \quad (18)$$

which after the localization equally expectedly gives

$$\hat{w}_t + \hat{\mathcal{J}}_x = 0.$$

ACTIVE DRIVING

Consider next a steadily propagating mechanical solitary wave (pulse) in the form of a traveling wave $u(x, t) = u(z)$, where $z = x - Dt$ with $D > 0$. We assume that it is driven internally by a chemical signal also in the form of a traveling wave, generating a dynamic active stress distribution $\sigma_a(x, t) = \sigma_a(z)$.

A reasonable assumption for living (or artificial) systems would be a continuous distribution σ_a , which would bring an additional length scale of chemo-diffusional nature into the model. However, for analytical simplicity, we here introduce a non-continuous distribution for σ_a . Specifically, we assume that the chemical activity wave can be represented by a combination of two mutually compensating rectangular pulses of compression and stretching:

$$\sigma_a(z) = \begin{cases} 0 & l < z \quad (\text{zone 1}) \\ -\sigma_0 & 0 < z < l \quad (\text{zone 2}) \\ \sigma_0 & -l < z < 0 \quad (\text{zone 3}) \\ 0 & z < -l \quad (\text{zone 4}) \end{cases} \quad (19)$$

where $\sigma_0 > 0$ is the amplitude of chemical activity and $2l$ is the size of the propagating activity zone, which so far is viewed as a parameter independent on D , the velocity of the

traveling wave. We must therefore integrate the resulting linear equation in the four domains separated by the discontinuities of σ_a .

Because the distribution of active stresses $\sigma_a(z)$ is piecewise constant, it is equivalent to a set of localized self-equilibrated forces (couples) generating active compression in $0 \leq z \leq l$ (zone 2) and active tension in $-l \leq z \leq 0$ (zone 2). In Fig. 2 we show schematically the active loading (19) for the pantographic structure in the case of a traveling wave solution.

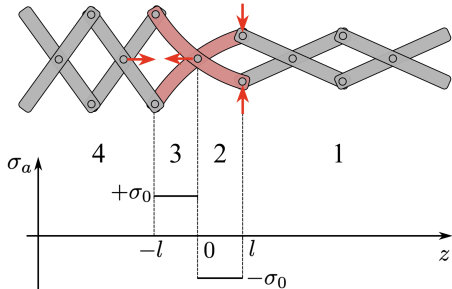


Figure 2. Schematic representation of the active loading (19) in the pantographic structure shown in Fig. 1. Note that active elements operate only inside the chemically active region.

TRAVELING WAVES

Traveling wave solutions are obtained by solving the fourth-order linear ODE

$$E_{\text{eff}}u''(z) - \kappa u'''(z) = -\sigma'_a(z), \quad (20)$$

where $u' = du/dz$ and the effective modulus is

$$E_{\text{eff}} = E - \rho D^2.$$

Here E is the elastic modulus, ρ the density, and D the wave speed. When $E = 0$, $E_{\text{eff}} = -\rho D^2 \leq 0$.

Interpreting the left-hand side of (20) as the Euler-Lagrange equation of a static problem with elastic energy

$$\int \left(\frac{1}{2} \kappa u_{xx}^2 + \frac{1}{2} E_{\text{eff}} u_x^2 \right) dx$$

we see that although $E > 0$, inertial effects can make $E_{\text{eff}} < 0$. This mechanism underlies the emergence of a buckling-type instability, that produces different types of traveling waves in the system, as we discuss below.

On the moving surfaces of discontinuity of the active field $\sigma_a(z)$, the solutions to (20) should be matched by using the corresponding jump conditions. When changing variables, the continuity conditions $\llbracket u \rrbracket = 0$, $\llbracket u_x \rrbracket = 0$ on the jumps become

$$\llbracket u \rrbracket = 0, \quad \llbracket u' \rrbracket = 0 \quad (21)$$

whereas the continuity of tractions and hypertractions on the jumps gives

$$\llbracket \sigma_a - \kappa u''' \rrbracket = 0, \quad \llbracket u'' \rrbracket = 0. \quad (22)$$

As it follows from (17) and (21)₁, the dissipation at a jump is

$$\mathcal{D} = D \llbracket \sigma_a \rrbracket u'. \quad (23)$$

Since $\llbracket \sigma_a \rrbracket$ differs from zero on such jump, the requirement that the soliton is non-dissipative is equivalent to the condition that

$$u' = 0 \quad (24)$$

at the jump. Finally, we observe that according to the general expression (13), the flux of energy for the stationary solution is

$$\mathcal{J}(z) = D \kappa u''^2(z) + D u'(z) \hat{\sigma}(z). \quad (25)$$

It will be convenient to work with dimensionless variables and we set

$$l_0 = \sqrt{\frac{\kappa}{\sigma_0}}, \quad c_0 = \sqrt{\frac{\sigma_0}{\rho}}$$

as the scales of length and velocity, respectively. The remaining main nondimensional parameters of the problem are then

$$K = \frac{l}{l_0}, \quad \nu = \sqrt{\frac{E}{\sigma_0}}.$$

In what follows we mark dimensionless variables with tildes,

$$\tilde{z} = \frac{z}{l_0}, \quad \tilde{u} = \frac{u}{l_0}, \quad \tilde{D} = \frac{D}{c_0}.$$

Then, with reference to (19), zone 1 corresponds to $K \leq \tilde{z}$, zone 2 to $0 \leq \tilde{z} \leq K$, zone 3 to $-K \leq \tilde{z} \leq 0$, and zone 4 to $\tilde{z} \leq -K$.

The simplicity of our setting allowed us to solve the problem analytically in its full generality. Depending on the values of the nondimensional parameters we identified two main regimes: supersonic and subsonic.

SUPersonic REGIME

Suppose first that the chemical driving impulse propagates with velocity

$$\tilde{D} \geq \nu. \quad (26)$$

It is natural to refer to this regime as supersonic. Note that one is always in this regime when “stretching” elasticity is negligible, meaning $E \approx 0$ and therefore effective sonic velocity ν is small.

In this regime the general solution of (20) in the regions 1-4 is a combination of linear and periodic functions,

$$u_a(z) = c_{a1} + c_{a2}z + c_{a3} \cos(\beta z/l_0) + c_{a4} \sin(\beta z/l_0) \quad (27)$$

where $a = 1, \dots, 4$. In (27) we introduced the notation

$$\beta = \sqrt{\tilde{D}^2 - \nu^2}.$$

Consider first solutions with compact support localized in the active region. To define such regimes we set

$$\tilde{u}_1(\tilde{z}) = \tilde{u}_4(\tilde{z}) = 0.$$

Under these constraints, the system (21),(22), (23) becomes over-determined and non-trivial solutions exist only at the special values of parameter β . Specifically, we obtain a discrete spectrum of admissible values

$$\beta_n = \frac{2l_0}{l} n\pi, \quad n = 1, 2, \dots \quad (28)$$

The corresponding *compactons* are of the form

$$\tilde{u}_{2,3}(\tilde{z}) = \frac{K^2}{8n^3\pi^3} \left(2n\pi(K \mp \tilde{z}) \pm K \sin\left(\frac{2n\pi\tilde{z}}{K}\right) \right). \quad (29)$$

The structure of these solutions is illustrated in Fig.3 for the smallest values of the integer parameter n . Note that they re-

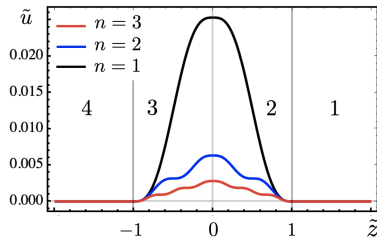


Figure 3. Dimensionless displacement field in compactons for different values of n . Here $K = 1$ and $-2 \leq \tilde{z} \leq 2$.

quire for their existence a very special values of the velocity of the active signal given by the formulas

$$D_n = \left(\left(\frac{2n\pi}{l} \right)^2 \frac{\kappa}{\rho} + \frac{E}{\rho} \right)^{1/2}. \quad (30)$$

Note, in particular, that D_n does not depend on the level of active prestress σ_0 and that narrow pulses (small l) move faster than broad ones (big l). More generally, the presence of a mechanical constraint on the spectrum of admissible velocities of chemical signals suggests that there is a feedback between mechanical and chemical systems. In this sense, the constructed compact pulses are truly “chemo-mechanical”.

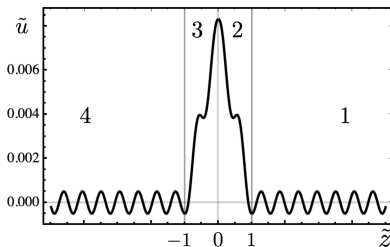


Figure 4. Dimensionless displacement field in (nanopterons) obtained for $\beta = 0.9\beta_2$. Here $K = 1$ and $-5 \leq \tilde{z} \leq 5$.

If we now relax the requirement that the displacements vanish in the regions 1 and 4, and instead impose the weaker condition that displacements remain bounded, we need to impose the constraints $c_{12} = c_{42} = 0$. If we also require that $c_{11} = c_{41} = 0$, so that the average displacements in the the regions 1 and 4 are equal to zero, we obtain unique solutions of the system (21), (22), and (23) for a continuous range of parameters $\beta > 0$ (including compactons as special cases) in the form

$$\tilde{u}_{1,4}(\tilde{z}) = \frac{\cos((K \mp \tilde{z})\beta) \tan\left(\frac{K\beta}{2}\right)}{\beta^3} \quad (31)$$

in zones 1, 4, and

$$\tilde{u}_{2,3}(\tilde{z}) = \frac{K\beta - \tilde{z}\beta + \sin(\tilde{z}\beta) - \cos(\tilde{z}\beta) \tan\left(\frac{K\beta}{2}\right)}{\beta^3} \quad (32)$$

in zones 2, 3, see a representative profile in Fig.4. Such semi-localized traveling waves with oscillatory tails reaching infinity are sometimes referred to as *nanoptera* or *nanopterons* [60–67]. The relation between nanopterons and compactons is illustrated in Fig. 5.

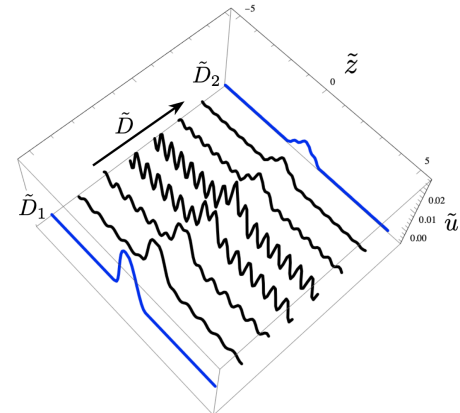


Figure 5. Solitary waves with periodic tails (nanopterons shown in black) in the interval of driving velocities between $\tilde{D}_1 = 2\pi/K$ and $\tilde{D}_2 = 4\pi/K$. The corresponding compactons at \tilde{D}_1 and \tilde{D}_2 are shown in blue. Here $K = 1$, $E = 0$.

In our case such solutions are characterized by nonzero energy radiation at $\pm\infty$ even though under the assumptions (31, 32) the energy loss or gain at the three jump discontinuities ($\mathcal{D}_{12} = \mathcal{D}_{23} = \mathcal{D}_{34} = 0$) is equal to zero. To assess the rate of energy exchange at infinity we can compute the period-averaged energy flux. Using the definition

$$\langle \mathcal{J} \rangle := \frac{\omega}{2\pi} \int_0^{2\pi/\omega} \mathcal{J}(z) dz \quad (33)$$

where ω is the angular frequency of a periodic signal we obtain that in our oscillatory tails (regimes 1 and 4)

$$\langle \mathcal{J}_1 \rangle = \langle \mathcal{J}_4 \rangle = \frac{c_0^2 D \rho (2\beta^2 + \nu^2)}{2\beta^4} \tan\left(\frac{l\beta}{2l_0}\right)^2. \quad (34)$$

One can see that these fluxes are different from zero unless the parameter β_n takes the discrete values given by (28). Therefore, the traveling waves described by (31)–(32) are not exchanging energy with $\pm\infty$ only at quantized velocity values given by . This also implies that only compact pulses are *self-sustaining* in the above sense.

Instead, as we show in Fig. 6 the noncompact supersonic nanopterons exhibit resonant behavior with diverging amplitude at

$$\beta_n^\infty = \frac{l_0}{l}(\pi + 2n\pi), \quad n = 0, 1, 2, \dots \quad (35)$$

This means, in particular, that in sharp contrast with self-sustaining compactons, the traveling pulses corresponding to (35) may exhibit arbitrary strong dependence on what is happening at infinity. For instance, the average fluxes in the tails (34) diverge for β corresponding to (35).

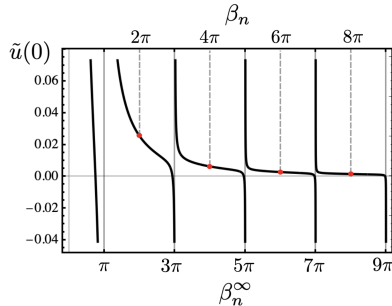


Figure 6. Amplitudes of the displacement field at $\tilde{z} = 0$ as a function of the coefficient β . The vertical asymptotes (resonant regimes) correspond to $\beta = \beta_n^\infty$ (they are marked at the lower horizontal axis); the values $\beta = \beta_n$ corresponding to compactons are marked on the upper horizontal axis. Here $K = 1$.

To answer the question about the direction of the energy exchange with infinity in nanopterons, for instance, to decide whether it is dissipative or anti-dissipative, we need to discuss the implied radiative energy transfer in more detail.

Note first that if we average the oscillatory solutions in the tails

$$\langle \mathcal{J} \rangle = D_g \langle w \rangle. \quad (36)$$

Here we introduced the group velocity

$$D_g = \frac{d\omega}{dk} \quad (37)$$

where $\omega(k)$ is the dispersion relation which is obtained substituting the ansatz $u(x, t) = e^{i(kx - \omega t)}$ into (14). We obtain

$$\omega^2 = c_0^2 \nu^2 k^2 + c_0^2 l_0^2 k^4$$

which gives

$$D_g = \frac{c_0(\nu^2 + 2l_0^2 k^2)}{k \sqrt{\nu^2 + l_0^2 k^2}}. \quad (38)$$

Observe next that in a traveling wave moving with velocity D , the emitted/received “effective phonons” propagate with the phase velocity

$$D_p = \frac{\omega}{k} = c_0 \sqrt{\nu^2 + l_0^2 k^2} = D. \quad (39)$$

One can see that

$$D < D_g < 2D$$

with D_g continuously interpolating between $D_g = 2D$ in the bending-dominated case ($\nu = 0$) and $D_g \rightarrow D$ in the extensional-dominated case ($\nu \rightarrow \infty$). In other words, the presence of stretching elasticity lowers the group velocity but never below the velocity of the pulse. Since, independently of the value of ν , the group velocity D_g remains strictly larger than D , the elastic energy is radiated ahead of the moving pulse. Therefore nanoptera solutions with two sided oscillatory tails will be able to dissipate energy at $+\infty$ while also being able to receive energy from sources at $-\infty$.

The developed understanding regarding the directionality of the radiative energy transfer can also shed light on the energetics behind the propagation of the quantized compactons. Note first that, in contrast to what we have concluded for nanopterons, for the steady propagation of the compact mechanical pulses it is necessary that around the internal boundary $\tilde{z} = K$, where the activity is switched on, energy is received, while around the internal boundary $\tilde{z} = -K$, where the activity is turned off, energy is released. Moreover, since for compactons

$$\mathcal{J}(z) = D_n w(z) \quad (40)$$

we can also conclude that in regions 2, 3 so $\mathcal{J}(z) \geq 0$ while $\mathcal{J}(z) = 0$ in regions 1,4.

Furthermore, since $D_g > D$, the energy travels faster than the pulse itself and therefore there exists a relative unidirectional energy transfer from the back of the pulse to its front. More specifically, the released mechanical energy at the rear of the pulse travels to the front of the pulse and the absorbed energy at the front is exactly equal to the released energy at the rear. Effectively, the system is harvesting the mechanical energy at one region and is relocating it with zero loss to another region. It is rather remarkable, that under this scenario, no chemical energy is needed to ensure the mechanical performance of the system. In this sense, while the chemical microscopic machinery still expends energy to generate the driving signal, the compact pulses can be viewed as mechanically autonomous.

SUBSONIC REGIME

Here we briefly discuss the subsonic traveling wave solutions of (20) corresponding to

$$\tilde{D} < \nu. \quad (41)$$

They require for their existence that either the stretching elasticity $E > 0$ is sufficiently big or the the velocity of the chemical signal \tilde{D} is sufficiently small. In such cases the general solution of the boundary value problem is the combination of linear and exponential functions,

$$u_a(z) = b_{a1} + b_{a2}z + b_{a3}e^{\alpha z/l_0} + b_{a4}e^{-\alpha z/l_0} \quad (42)$$

where $a = 1, \dots, 4$ and where we have set

$$\alpha = \sqrt{\nu^2 - \tilde{D}^2}.$$

Under the assumptions

$$b_{11} = b_{12} = b_{13} = b_{41} = b_{42} = b_{44} = 0$$

the solution decays at $\pm\infty$ as desired. By imposing the jump conditions (21), (22), we obtain a one parametric family of the solutions. Specifically, using α as the parameter, we obtain that in dimensionless variables the solution in zones 1, 4 is

$$\tilde{u}_{1/4}(\tilde{z}) = -\frac{(e^{K\alpha} - 1)^2}{2\alpha^3} e^{-\alpha(K \pm \tilde{z})} \quad (43)$$

whereas in zones 2,3 it is

$$\tilde{u}_{2/3}(\tilde{z}) = \frac{e^{\mp\alpha\tilde{z}} - e^{-\alpha K} \cosh(\alpha\tilde{z})}{\alpha^3} - \frac{K \mp \tilde{z}}{\alpha^2}. \quad (44)$$

In Fig.7 we illustrate the typical profiles (43,44) corresponding to different values of \tilde{D} . In striking contrast to the supersonic compactons shown in Fig. 3 and characterized by the condition $\tilde{u} \geq 0$, the compact subsonic pulses (43,44) have instead $\tilde{u} \leq 0$.

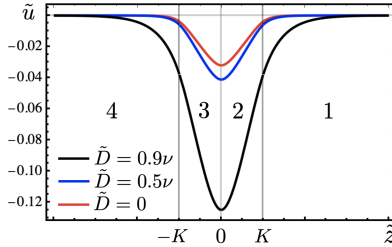


Figure 7. Dimensionless displacement field in the subsonic regime with $\nu = 5$ and different values of the velocity \tilde{D} .

This is related to the fact that while in the supersonic case we deal with anomalous negative effective stiffness $E_{\text{eff}} < 0$, in the subsonic case we are in a more conventional regime with $E_{\text{eff}} > 0$. To see the implication of this it is sufficient to observe that at $\tilde{D} = 0$ the static version of the solution (43,44) can be interpreted as the classical buckling of a beam induced by a distributed pre-stress, see for instance [68, 69]. In particular, our static solution shows that in regions of active internal tension (zone 3, where $\sigma_a > 0$), the system exhibits *shortening* ($\tilde{u}' < 0$), whereas in regions of active internal contraction (zone 2, where $\sigma_a < 0$), it shows *extension* ($\tilde{u}' > 0$). This behavior persists throughout the subsonic regime but changes

qualitatively in the supersonic regimes where the $\tilde{u}(\tilde{z})$ profiles flip over due to the emergence of negative stretching elasticity. Note also that when the parameter \tilde{D} approaches the critical value ν from any of the two sides sides $\tilde{D} \leq \nu$, which in dimensional variables means that the chemical signal reaches the critical velocity

$$D = c_0 \sqrt{\frac{E}{\sigma_0}} \quad (45)$$

the magnitude of the displacement field diverges. As many other critical regimes of this type, the limit (45) may be of particular biological relevance, see for instance [70–72]

Finally we mention that subsonic pulses do not interact energetically with $\pm\infty$ since the fluxes

$$\mathcal{D}_{1/4} = \frac{\varrho \tilde{D} c_0^3 \nu^2}{4(\tilde{D}^2 - \nu^2)^2} \left(e^{K\sqrt{\nu^2 - \tilde{D}^2}} \right)^4 e^{-2(K \pm \tilde{z})} \quad (46)$$

vanish inside the exponential tails. Also the global dissipation is zero, due to the exact cancellation between the energy sink at the dissipative singularity located at the leading edge of the active region (the jump separating regions 1 and 2) and energy source located at the anti-dissipative singularity at the corresponding trailing edge (the jump separating regions 3 and 4)

$$\mathcal{D}_{12} = -\mathcal{D}_{34} = \frac{c_0^3 \tilde{D} \rho}{2(\nu^2 - \tilde{D}^2)} \left(1 - e^{-K\sqrt{\nu^2 - \tilde{D}^2}} \right)^2. \quad (47)$$

Given that $\mathcal{D}_{23} = 0$ which means that there are no energy sources or sinks between regions 2 and 3, we can conclude that $\mathcal{D} = \mathcal{D}_{12} + \mathcal{D}_{23} + \mathcal{D}_{34} = 0$ and that as long as the local sources and sinks are balanced, the corresponding mechanical system is energetically autonomous.

DISCUSSION

We have seen that the velocity of compact supersonic chemo-mechanical solitons, which are the only relevant ones in the physically realistic regime when stretching elasticity is negligible, can only take a discrete set of values. Instead, a generic chemical driving would have produced a highly dissipative mechanical response with energy escaping to infinity due to unavoidable generation of elastic radiation by the advancing mechanical pulse. The cancellation of such radiative damping through a particular choice of the chemical signal can be achieved only due to self organization implying an intricate coupling between chemistry and elasticity. In our highly schematic model such coupling is characterized by a dimensionless quantity K which brings together the parameters of the chemical activation (l, σ_0) and the elastic modulus κ . While in the context of biological systems, the special regimes exhibiting compact pulses (whose stability is to be addressed separately), can be viewed as a result of evolution, it is clear that artificial robotic systems of the same type can be directly controlled to exclude or at least minimize radiation by parasitic elastic waves.

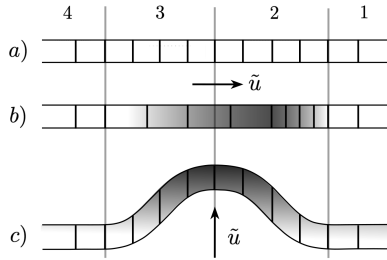


Figure 8. Schematic representation of a mechanical pulse advancing to the right. *a*) Reference (undeformed) configuration; *b*) deformed configuration in the case of longitudinal displacements; *c*) deformed configuration in the case of transverse displacements. The intensity of gray is proportional to the magnitude of displacement.

One possible physical interpretation of the obtained quantized compact pulses can be in terms of a model of a peristaltic “pump”. To this end consider a compacton configuration with the largest amplitude, which corresponds to $n = 1$. Then, instead of viewing it as representing a longitudinal deformation, driven by localized tension and compression, suppose that it represents a transverse deformation, driven by active chemical pulse inducing a combination of positive and negative shear as it is schematically illustrated in Fig. 8. In this case the resulting deformation takes the form of a localized “bulge” propagating along a beam placed without cohesion on a flat surface. The beam need of course to be dynamically pre-stressed by a chemical signal. The leading edge of the propagating bulge would then represent the tip of an opening “crack”, while the trailing edge would indicate the location of its closure side. Interestingly, a concept of such self-healing mechanical propagation of a localized pulse is used in non-biological fields as well fields from friction to earthquakes [73, 74].

Another relevant analogy would be with mechanical solitary waves in nonlinear dispersive passive systems. Since the corresponding localized wave packets are energy conserving, they necessarily support an internal energy transfer between the leading and the trailing segments. For instance, in the case of discrete FPU-type solitons, one can interpret the leading edge as a partially developed *admissible* shock wave while the trailing segment can be similarly viewed as an *non-admissible* shock wave [75]. While in such problems the nature of dispersion is different from our case so that, in particular, the energy transport takes place from the front to the back so that the “dissipative” shock “feeds” (and in this way stabilizes) the “anti-dissipative” one [34, 76].

CONCLUSIONS

In this paper we considered a simple continuum model illustrating a possibility of chemically activated mechanical motion in biological systems. The crucial idea was to represent chemical degrees of freedom by an external stress field. Our main result is the development of a prototypical model of a chemo-mechanical soliton driven by a passive-to-active

transformation at the front and a matching active-to-passive transformation at the rear. We showed that such solitons can be generated by dynamic inhomogeneities even in the simplest *linear* mechanical systems. The obtained pulse solutions can be interpreted as describing spatially distributed chemo-mechanical motors converting mechanically neutral chemical signals into functional mechanical activity. There is a considerable interest to reproduce such biological mechanisms artificially in soft robots [77–80], and in this sense the proposed model can serve as a proof of concept. Thus, while the model predicts energy transfer with perfect efficiency one should have in mind that we neglected some sources of dissipation in the bulk including the ones associated with reaction-diffusion driving as well as mechanical friction. Therefore future work aimed at fully quantitative designs should also account for dissipation. The comprehensive study must also account for the functional work (cargo) and should be set in a realistic 3D geometry.

ACKNOWLEDGMENTS

The authors thank P. Recho, A. Vainchtein, G. Mishuris and N. Gorbushin for helpful discussions. L.T. acknowledges the support under the grants ANR-17-CE08-0047-02 and ANR-21-CE08-MESOCRYSP.

- [1] T. Savin, N. A. Kurpios, A. E. Shyer, P. Floreescu, H. Liang, L. Mahadevan, and C. J. Tabin, *Nature* **476**, 57 (2011).
- [2] E. Coen and D. J. Cosgrove, *Science* **379**, eade8055 (2023).
- [3] P. Lappalainen, T. Kotila, A. Jégou, and G. Romet-Lemonne, *Nature Reviews Molecular Cell Biology* **23**, 836 (2022).
- [4] L. Truskinovsky, G. Vitale, and T. Smit, *International Journal of Engineering Science* **83**, 124 (2014).
- [5] B. Slater, W. Jung, and T. Kim, *Cytoskeleton* (2023).
- [6] B. Wang and Y. Lu, *Nano-Micro Letters* **16**, 155 (2024).
- [7] C. Bagshaw, *Muscle contraction* (Springer Science & Business Media, 1993).
- [8] C. Lindemann and K. Lesich, *Cytoskeleton* (2024).
- [9] M. Beeby, J. Ferreira, P. Tripp, S.-V. Albers, and D. Mitchell, *FEMS Microbiology Reviews* **44**, 253 (2020).
- [10] X. Serra-Picamal, V. Conte, R. Vincent, E. Anon, D. Tambe, E. Bazellieres, J. Butler, J. Fredberg, and X. Trepat, *Nature Physics* **8**, 628 (2012).
- [11] D. Boocock, N. Hino, N. Ruzickova, T. Hirashima, and E. Hananezo, *Nature Physics* **17**, 267 (2021).
- [12] M. Sinnott, P. Cleary, and S. Harrison, *Applied Mathematical Modelling* **44**, 143 (2017).
- [13] K. Quillin, *Journal of Experimental Biology* **202**, 661 (1999).
- [14] N. Gorbushin and L. Truskinovsky, *Physical Review E* **103**, 042411 (2021).
- [15] L. Pismen, *Patterns and interfaces in dissipative dynamics*, Vol. 706 (Springer, 2006).
- [16] F. Pérez-Verdugo, S. Banks, and S. Banerjee, *Communications Physics* **7**, 167 (2024).
- [17] A. Kindberg, J. Hu, and J. Bush, *Current Opinion in Cell Biology* **66**, 59 (2020).

[18] F. Alisafaei, X. Chen, T. Leahy, P. Janmey, and V. Shenoy, *Soft Matter* **17**, 241 (2021).

[19] D. Dean, A. Nain, and G. Genin, *Mechanics of cells and fibers* (2023).

[20] G. Livne, S. Gat, S. Armon, and A. Bernheim-Groswasser, *Proceedings of the National Academy of Sciences* **121**, e2309125121 (2024).

[21] I. Levin, R. Deegan, and E. Sharon, *Physical Review Letters* **125**, 178001 (2020).

[22] R. K. Manna, K. Gentile, O. E. Shklyaev, A. Sen, and A. C. Balazs, *Langmuir* **38**, 1432 (2022).

[23] D. Duffy, I. Griniasty, J. Biggins, and C. Mostajeran, in *Proceedings A*, Vol. 481 (The Royal Society, 2025) p. 20240387.

[24] S. Li, D. A. Matoz-Fernandez, A. Aggarwal, and M. Olvera de la Cruz, *Proceedings of the National Academy of Sciences* **118**, e2025717118 (2021).

[25] S. Sarkar, B. Ash, Y. Wu, N. Boechler, S. Shankar, and X. Mao, *arXiv preprint arXiv:2505.18272* (2025).

[26] A. Zakharov and K. Dasbiswas, *Soft Matter* **17**, 4738 (2021).

[27] O. Y. Cohen, Y. Klein, and E. Sharon, *arXiv preprint arXiv:2402.16112* (2024).

[28] S. Yin, B. Li, and X. Q. Feng, *Proceedings of the National Academy of Sciences* **119**, e2206159119 (2022).

[29] X. Q. Feng, B. Li, S. Z. Lin, M. Y. Wang, X. D. Chen, H. X. Zhang, and W. Fang, *Acta Mechanica Sinica* **41**, 625315 (2025).

[30] R. C. Ihuaenyi, H. Zhao, R. Fang, R. Bai, M. Z. Bazant, and J. Zhu, *arXiv preprint arXiv:2508.17523* (2025).

[31] J. R. Picardo, V. Jemseena, and K. V. Kumar, *Physical Review E* **112**, L022401 (2025).

[32] Y. Xiong, A. Aggarwal, and M. Olvera de la Cruz, *Advanced Functional Materials*, 2507078 (2025).

[33] Y. Kartashov, B. Malomed, and L. Torner, *Reviews of Modern Physics* **83**, 247 (2011).

[34] L. Truskinovsky and A. Vainchtein, *Physical Review E* **90**, 042903 (2014).

[35] Y. Ming, L. Ye, H.-S. Chen, S.-F. Mao, H.-M. Li, and Z.-J. Ding, *Physical Review E* **97**, 012221 (2018).

[36] O. Dudchenko and G. Guria, *Physical Review E* **85**, 020902 (2012).

[37] D. Ambrosi and S. Pezzuto, *Journal of Elasticity* **107**, 199 (2012).

[38] E. Brunello and L. Fusi, *Annual Review of Physiology* **86**, 255 (2024).

[39] M. Caruel and L. Truskinovsky, *Reports on Progress in Physics* **81**, 036602 (2018).

[40] J. Prost, F. Jülicher, and J.-F. Joanny, *Nature Physics* **11**, 111 (2015).

[41] K. Kruse, J.-F. Joanny, F. Jülicher, J. Prost, and K. Sekimoto, *The European Physical Journal E* **16**, 5 (2005).

[42] I. Levin, R. Deegan, and E. Sharon, *Phys. Rev. Lett.* **125**, 178001 (2020).

[43] G. Livne, S. Gat, S. Armon, and A. Bernheim-Groswasser, *Proceedings of the National Academy of Sciences* **121**, e2309125121 (2024).

[44] S. Li, D. A. Matoz-Fernandez, A. Aggarwal, and M. O. de la Cruz, *Proceedings of the National Academy of Sciences* **118**, e2025717118 (2021).

[45] G. Whitham, *Linear and nonlinear waves* (John Wiley & Sons, 2011).

[46] O. Kresse and L. Truskinovsky, *Journal of the Mechanics and Physics of Solids* **52**, 2521 (2004).

[47] L. Slepyan, *Models and phenomena in fracture mechanics* (Springer Science & Business Media, 2012).

[48] N. Gorbushin, G. Mishuris, and L. Truskinovsky, *Physical Review Letters* **125**, 195502 (2020).

[49] M. Schenk and S. D. Guest, *Proceedings of the Institution of Mechanical Engineers, Part C: Journal of Mechanical Engineering Science* **228**, 1701 (2014).

[50] J.-J. Alibert, P. Seppecher, and F. Dell'Isola, *Mathematics and Mechanics of Solids* **8**, 51 (2003).

[51] C. Boutin, J. Soubestre, M. S. Dietz, and C. Taylor, *European Journal of Mechanics-A/Solids* **42**, 280 (2013).

[52] M. Camar-Eddine and P. Seppecher, *Archive for Rational Mechanics and Analysis* **170**, 211 (2003).

[53] L. Mahadevan and P. Matsudaira, *Science* **288**, 95 (2000).

[54] M. Badoual, F. Jülicher, and J. Prost, *Proceedings of the National Academy of Sciences* **99**, 6696 (2002).

[55] S. Gavrilyuk, B. Nkonga, K.-M. Shyue, and L. Truskinovsky, *Nonlinearity* **33**, 5477 (2020).

[56] R. D. Mindlin and H. Tiersten, *Archive for Rational Mechanics and Analysis* **11**, 415 (1962).

[57] R. A. Toupin, *Archive for Rational Mechanics and Analysis* **17**, 85 (1964).

[58] J. Eshelby, *Journal of Elasticity* **5**, 321 (1975).

[59] L. Truskinovskii, *Journal of Applied Mathematics and Mechanics* **51**, 777 (1987).

[60] J. T. Beale, *Communications on Pure and Applied Mathematics* **XLIV**, 211 (1991).

[61] J. P. Boyd, *Physica D: Nonlinear Phenomena* **48**, 129 (1991).

[62] A. J. Moston-Duggan, M. A. Porter, and C. J. Lustri, *Journal of Nonlinear Science* **33**, 12 (2023).

[63] T. E. Faver, *Quarterly of Applied Mathematics*, 1548 (2019).

[64] T. E. Faver and H. J. Hupkes, *Partial Differential Equations in Applied Mathematics* **4**, 100128 (2021).

[65] A. Vainchtein, *Physica D: Nonlinear Phenomena* **434**, 133252 (2022).

[66] E. Kim, F. Li, C. Chong, G. Theocaris, J. Yang, and P. G. Kevrekidis, *Physical Review Letters* **114**, 118002 (2015).

[67] J. Widjaja, Y. L. Qiang, A. F. J. Skelton, L. H. H. Sweetland, A. F. J. Runge, C. J. Lustri, and C. M. de Sterke, *Nature Communications* **16**, 60555 (2025).

[68] R. Paroni and G. Tomassetti, *Mathematics and Mechanics of Solids* **20**, 982 (2015).

[69] X. Ren and S. Shi, *Materials* **16**, 6390 (2023).

[70] T. Mora and W. Bialek, *Journal of Statistical Physics* **144**, 268 (2011).

[71] M. A. Munoz, *Reviews of Modern Physics* **90**, 031001 (2018).

[72] A. Hudspeth and P. Martin, *Journal of Neuroscience* **44** (2024).

[73] G. Perrin, J. R. Rice, and G. Zheng, *Journal of the Mechanics and Physics of Solids* **43**, 1461 (1995).

[74] K. Thøgersen, E. Aharonov, F. Barras, and F. Renard, *Physical Review E* **103**, 052802 (2021).

[75] C. M. Dafermos, *Hyperbolic conservation laws in continuum physics*, Vol. 3 (Springer, 2005).

[76] A. Vainchtein and L. Truskinovsky, *arXiv preprint arXiv:2405.09302* (2024).

[77] D. Agostinelli, F. Alouges, and A. DeSimone, *Frontiers in Robotics and AI* **5**, 99 (2018).

[78] P. W. Miller and J. Dunkel, *Soft Matter* **16**, 3991 (2020).

[79] C. Pehlevan, P. Paoletti, and L. Mahadevan, *Elife* **5**, e11031 (2016).

[80] P. Recho and L. Truskinovsky, *arXiv preprint arXiv:2406.06437* (2024).